An 8Gbps Adaptive Receiver for RF over FSO in 28nm CMOS

Fatemeh Aghlmand, Saransh Sharma, Azita Emami
Electrical Engineering Department, California Institute of Technology, USA
aghlmand@caltech.edu, ssharma3@caltech.edu, azita@caltech.edu

***Abstract* — This paper presents a fully integrated high-bandwidth receiver for RF-over-free-space optics (RoFSO). Using subcarrier intensity modulation (SIM) and direct detection scheme, high data rate optical communication is supported in a high-loss atmospheric channel. For proof-of-concept demonstration, an 8Gbps input data via differential phase shift keying (DPSK) modulation and with 10GHz of RF bandwidth is employed. The link performance is assessed by exposing the system to more than 26dB of optical loss equivalent to 3.5km of free space distance under moderate visibility conditions. The receiver chip uses adaptive control loops to compensate for the atmospheric effects and extends the dynamic range. It has been designed and implemented in 28nm CMOS process and achieves 58dB of gain and 18GHz of bandwidth.**

***Keywords* — RF-over-free-space, subcarrier intensity modulation, differential phase shift keying.**

I. Introduction

The ever-increasing demand for higher data rate communication has drawn significant attention to transmission of high-speed RF signals over optics. RF over fiber (RoF), RF over free space optics (RoFSO) and Hybrid RF/Optics are three major approaches with specific applications and challenges.

With recent advances in digital signal processing (DSP), phase-modulated RoF links with coherent receivers have shown promising results [1]. However, in dense urban areas and remotely located settlements where the installation of optical fiber infrastructure is costly and time consuming, RoFSO has shown to be a superior candidate. Furthermore, for space to ground, ground to space and inter-satellite links, RoFSO is the preferred choice with its high security (immunity to electromagnetic interference), directivity (no multipath fading) and abundance of unregulated RF bandwidth, (Fig. 1).

For the most challenging link, i.e. space to ground, the weak optical wave enters the earth's atmosphere and faces turbulence effects which are caused by the air refractive-index random fluctuations. Consecutively, the wavefront propagates in the atmospheric channel with variable speed leading to sever phase distortion. Hence, adaptive optics is required at the ground station to reduce beam aberration. On the other hand, natural factors (fog, rain, etc.) cause high attenuation and variation of the received optical intensity (scintillation). Using bigger aperture size (i.e. aperture averaging) at the ground reduces variation of the received optical power at the expense of higher cost and larger space (Fig. 2). Therefore, designing a wide dynamic range optical receiver will greatly relax the aperture

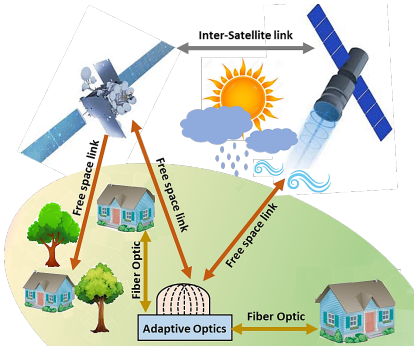

Fig. 1. Free space optical communication

size requirement for a cost-effective solution. Most of the reported works for RF over optics applications are experimental setups using off-the-shelf components to indicate feasibility of the link [1-3]. Utilizing both intensity and phase modulation as well as polarization multiplexing, [1] shows transmission of 4×2.5Gbps RF signals over 10km fiber. Coherent receiver and DSP are employed to eliminate the local laser's phase noise, resulting in BER of 10^{-3} for a minimum received power of -18dBm. A combined RoF and RoFSO system is presented in [2] to transmit the 64-QAM LTE-A signal with 100MHz of RF bandwidth, showing acceptable results over 12dB FSO loss. Another work describes a millimetre-wave (mmW) and FSO hybrid system for transmission of 4Gbps 16QAM signal [3]. Improved performance is reported for the hybrid link as FSO and mmW links exhibit complementary transmission characteristics under various weather conditions.

In this paper, we present a CMOS integrated optical receiver with wide dynamic range to withstand large variation of both average and peak optical power, required when using a significantly smaller aperture size. In this work, we have shown up to 8Gbps of successful data recovery from a minimum received power of -30dBm while using an optical amplifier.

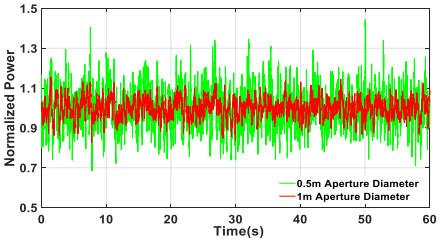

Fig. 2. Simulated scintillation effect from two aperture sizes

2020 15th European Microwave Integrated Circuits Conference (EuMIC) | 978-2-87487-060-6/21/$31.00 ©2021IEEE | DOI: 10.23919/EuMIC48047.2021.00024

The rest of this paper is organized as follows. Section II presents the system level design including modulation techniques and noise analysis. Integrated circuit design details are discussed in Section III. Measurement results for the prototype chip are described in section IV, and conclusions in Section V.

II. System Level Design

A. Modulation

To transmit an RF signal through atmospheric channel, the choice of modulation method is very important. High data rate RoF systems are reported with optical intensity/phase modulation and coherent detection [1]. Besides being complex in the optical and DSP domain due to the optical carrier recovery and phase estimation, the main requirement of this method is to have a perfectly coherent optical beam. Since atmospheric turbulence greatly reduces coherency of the beam, using phase modulation for FSO is impractical.

Subcarrier intensity modulation (SIM) is a promising method in which a phase-modulated RF carrier modulates the intensity of the optical beam, resulting in both average and peak optical power being constant. This is essential in a high scintillation channel since the information in the intensity of the beam would be lost. The choice of modulation technique at the subcarrier level requires a trade-off between complexity, power and bandwidth efficiencies. Differential PSK (DPSK) is selected in this work to avoid complex DSP for absolute RF phase estimation. Non-coherent demodulation of DPSK is done by comparing the phase of the received signal in any signaling interval with the preceding one. This is feasible in the turbulence condition since, as shown in Fig. 2, atmospheric channel coherence time (~msec) is long enough compared to the typical duration of two consecutive data bits in Gbps range.

B. Noise Analysis

The implemented system is shown in Fig. 3. Due to the weak received optical intensity, a combination of optical amplifier (EDFA) and PIN photodiode (PD) is required at the receiver. Defining the carrier to noise ratio (CNR) at the input of TIA, (1) shows the ratio of the photocurrent power to the sum of the various integrated noise components. Shot noise of the PD, RIN noise of the laser, thermal noise of the CMOS chip and amplified spontaneous emission (ASE) noise of the EDFA are the most important noise sources [4]. ASE noise as defined in

$$CNR = \frac{½\,(G\,\beta\,R\,P_0)^2}{\left[2qRGP_0 + RIN\,(RGP_0)^2 + I^2_{n,in} + I^2_{n,ASE}\right]BW_{RF}} \quad (1)$$

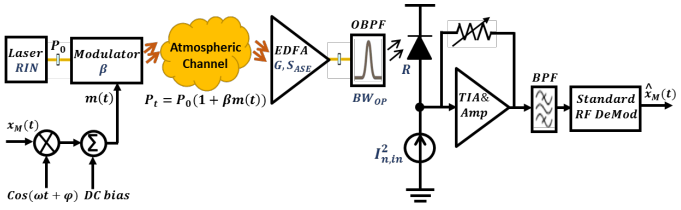

Fig. 3. System level illustration of the FSO link using SIM

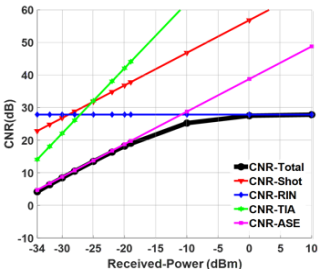

Parameter	Value
BW_{RF}	10 GHz
β	0.33
F_n	5dB
Wavelength	1550 nm
BW_{op}	0.1nm
Laser RIN	-140 dBc/Hz

Fig. 4. (a) Partial CNRs due to noise components (b) Key system parameters

(2) has two parts, Signal-ASE noise (dominant term) and ASE-ASE beat noise. To evaluate the effect of each noise source independently, partial CNRs due to each noise component are plotted in Fig. 4a. It is shown that for low received optical power, the most dominant noise of the system is ASE noise, resulting in quantum-limited CNR_{QL} as defined in (4). Hence, the most important parameters in the system are identified as intensity modulation depth (β), noise factor of EDFA (F_n), bandwidth of the RF signal (BW_{RF}) and the optical bandpass filter (BW_{op}). Fig. 4b. shows the selected system parameters.

$$I^2_{n,ASE} = R^2\left(2GP_0S_{ASE} + S^2_{ASE}BW_{op}\right) \quad (2)$$

$$S_{ASE} = (G-1)\left(\frac{hc}{\lambda}\right)F_n \quad (3)$$

$$CNR_{QL} = \frac{\frac{1}{4}\beta^2P_0}{F_n\left(\frac{hc}{\lambda}\right)BW_{RF}\left(1 + F_n\left(\frac{hc}{\lambda}\right)\frac{BW_{op}}{2P_0}\right)} \quad (4)$$

III. Circuit Design

The designed optical receiver schematic is shown in Fig. 5 It is implemented in TSMC 28nm CMOS technology, with supply voltage of 1.2V and current consumption of 16mA, excluding the 50Ω output buffer stage.

A front-end current buffer with the regulated cascode (RGC) structure is used to ensure very low input impedance seen by the PD parasitic cap. As mentioned earlier, the system noise is dominated by ASE noise of the EDFA, hence the main goal of the first electrical stage is to have minimum input impedance with the least power consumption. In the RGC circuit, addition of an amplifier (M_3, R_3) in the feedforward path with a level-shift circuit (M_2, R_2), reduces the input impedance of the circuit ($1/gm_1$) by a factor of $1 + gm_3R_3.gm_2R_2$ while leaving sufficient headroom at node V_x [5].

The RGC stage is followed by a voltage-controlled inverter-based TIA, which provides the negative input (V_n) for the single-ended to differential (STD) conversion in the next block. Using the inverter input node for STD rather than a replica TIA, provides larger swing and lower noise while saving power and area [6]. The gain control part is realized as a constant resistor in parallel with a PMOS and two series resistances. At high input signal level, the V_{AGC} is low, the PMOS is ON and the gain is set by its ON-resistance. Since the non-linearity of this PMOS may appear for large input swings, two series resistances are

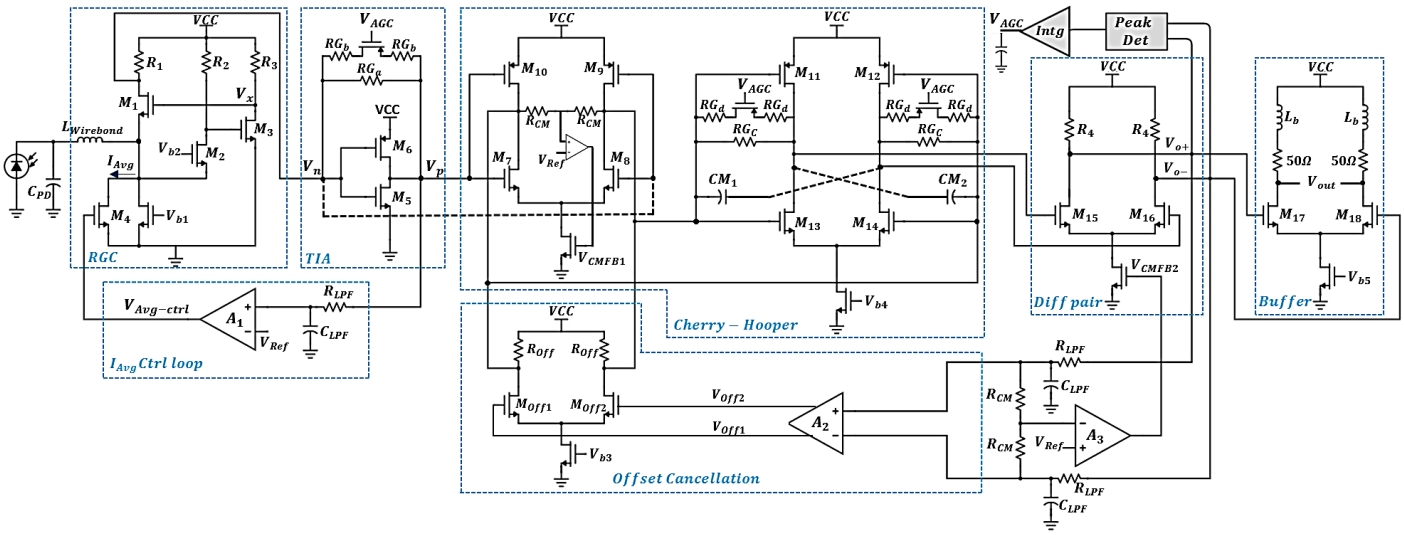

Fig. 5. Schematic of the integrated optical receiver

used to improve the linearity of this combination. In the case of large input photocurrent, the RGC gets saturated and causes signal distortion from early stages. Hence, the average PD current should be subtracted from the RGC input node. The output voltage of the TIA (V_p) is a suitable reference point for the average photocurrent control loop. Using a compact low-pass filter and the error amplifier A_1, $V_{Avg-ctrl}$ is generated for the voltage-controlled current source M_4.

To amplify the signal differentially while keeping the receiver wideband, a variable gain amplifier (VGA) based on the Cherry-Hopper (CH) circuit [7] is designed. It is composed of a differential trans-admittance (TAS) stage which converts the TIA voltage to current and a differential variable-gain transimpedance stage for I-to-V conversion. The gain of the VGA is determined by gm of the TAS and variable RG_c of the transimpedance. The two small negative Miller capacitances, ($CM_{1,2}$) decrease the total cap seen at the TAS output nodes.

Finally, a differential gain stage is implemented, and its outputs ($V_{o+/-}$) are used for the peak detection circuit required for the automatic gain control (AGC) loop. The peak detector is a source-follower pair which supplies the peak signal to the integrator block. Furthermore, the offset cancellation loop receives the average of $V_{o+/-}$ as the input, and after amplification by A_2, uses a differential GM stage ($M_{off1,2}$) to draw the corrective currents from the TAS circuit. Since the CH structure ensures low impedance at the TAS output nodes, additional loading by the offset cancellation circuit does not deteriorate the frequency response of the receiver. At the end, a 50Ω buffer stage with inductive peaking is designed to interface the chip with the measurement equipment.

IV. Measurement Results

The measurement setup is shown in Fig. 6. The 8Gbps DBPSK RF signal with RF bandwidth of 10GHz (pulse-shaping roll-off factor of 0.25) is generated using an arbitrary waveform generator. After amplification by a gain block, the RF signal is

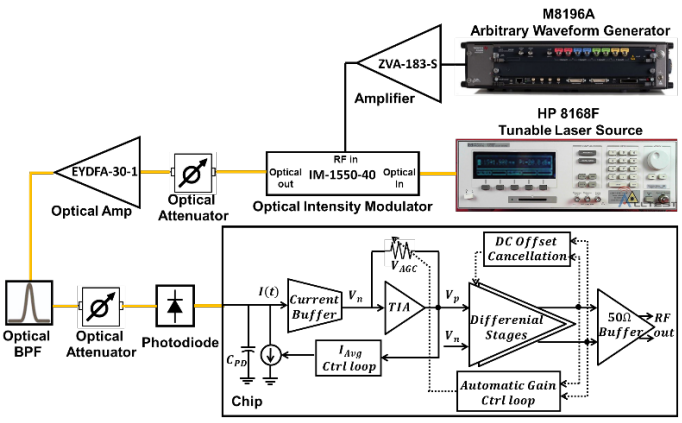

Fig. 6. Measurement setup

sent to the MZI optical intensity modulator to modulate the laser beam with 1dBm average power at 1550nm. To characterize the link tolerance to optical attenuation due to atmospheric effects, a variable optical attenuator is used before the EDFA. After the optical bandpass filter (to limit the ASE noise), another attenuator is used to model the possible long fiber loss. The PD is a 16μm-detection-window InGaAs PIN chip with 0.7A/W responsivity and 80fF capacitance. It is wirebonded to the input pad of the designed CMOS chip. The photodetected RF current passes through the RGC and variable gain stages to provide differential RF voltage, which is then processed in MATLAB for demodulation and BER calculations.

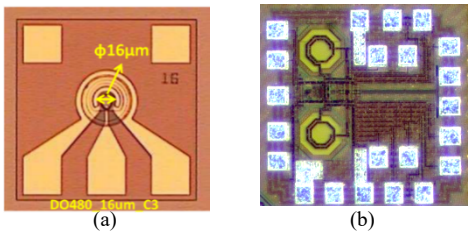

(a) (b)

Fig. 7. (a) Photodiode and (b) Receiver chip micrograph

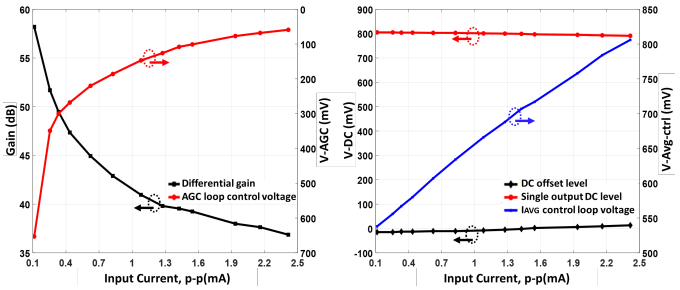

(a) (b)

Fig. 8. (a) AGC loop and (b) Average current control loop

The PD and receiver chip micrograph are shown in Fig. 7. The area of the chip is 0.6×0.6 mm^2, as dictated by the pad count.

Fig. 8a and b show the measured AGC loop and the average current control loop functionality, respectively. As the input current changes from 0.1mA to 2.4mA, differential gain varies over 21dB to limit output level variation to 5.2dB. The offset cancellation loop and the average current control loop work together to keep the DC value of the outputs near optimum level, with lower than ±15mV offset.

The measured frequency response of the chip after compensating the optical modulator's frequency response is shown in Fig. 9a. The 3dB frequency is around 18GHz, with flat frequency band of 3-13GHz for the 8Gbps DBPSK signal transmission. The BER as a function of the received power at the input of the optical amplifier, is shown in the Fig. 9b. For the received power of -28dBm and 8Gbps DBPSK data, the measured BER is 1×10^{-4} without applying any error correction codes. The BER improves as the data rate decreases or input power increases. Increasing depth of intensity modulation (β) has a great impact on attaining high CNR as shown in (4). However, higher β leads to more nonlinearity in the optical modulator. By biasing the modulator at the optimum point to minimize second harmonic and filtering the higher order distortions, better error performance is achieved for a single channel wideband signal. Sample constellation diagrams and spectrum of the DPSK RF signals are shown in Fig. 10.

Table I compares this work with previous RF over optics publications, none of which include integrated CMOS receivers. This design achieves a wide dynamic range operation with high optical attenuation and good BER while using non-coherent DPSK as subcarrier modulation. DPSK is used to reduce complexity while having 3dB CNR penalty compared to coherent PSK, which can be utilized to further decrease BER.

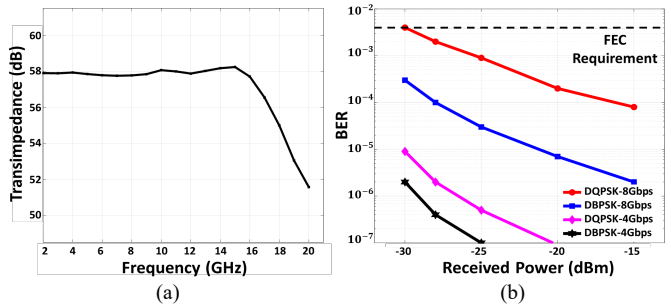

(a) (b)

Fig. 9. (a) Measured frequency response of the CMOS chip and (b) BER versus received optical power at different data rates

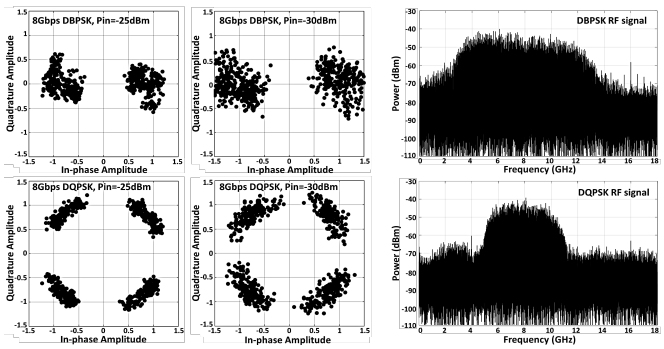

(a) (b)

Fig. 10. (a) Constellation diagrams and (b) Spectrum of the DPSK RF signals

Table 1. Comparison of performance parameters of RF over optics systems

Ref.	Appl.	Mod.	DR(Gbps)	Rec. power	BER
[1]	RoF	16QAM	4×2.5	-18dBm	1×10^{-3}
[2]	RoF/ RoFSO	SIM (64QAM)	0.6	-21dBm	2×10^{-3}
[3]	mmW/ RoFSO	SIM (16QAM)	4	-29dBm	1×10^{-5}
This work	RoFSO	SIM (DBPSK)	8	-28dBm	1×10^{-4}

V. Conclusion

This paper describes an integrated optical receiver system for RF over optics application. Using SIM, an RF signal is transmitted in high optical attenuation condition. A wideband CMOS receiver chip is designed with multiple controlling loops to increase the dynamic range. An 8Gbps non-coherent DPSK signal with RF bandwidth of 10GHz is transmitted, resulting in a BER of 1×10^{-4} while consuming 19.2mW power at the receiver. Future work can improve BER by using coherent modulation for subcarrier or using subcarrier diversity scheme with single optical front-end and multiple RF channels.

Acknowledgment

The authors would like to acknowledge Boeing for funding. We thank A.H. Talkhooncheh, K.-C. Chen (MICS lab) and M. Wright, S. Piazzolla (JPL) for helpful discussions.

References

[1] X. Chen and J. Yao, "Data Rate Quadrupled Coherent Microwave Photonic Link," in *IEEE Photonics Technology Letters*, vol. 29, no. 13, pp. 1071-1074, 1 July1, 2017.

[2] J. Bohata *et al.*, "24–26 GHz radio-over-fiber and free-space optics for fifth-generation systems," in *Opt. Lett.*, vol. 43, no. 5, pp. 1035–1038, Mar. 2018.

[3] J. Zhang *et al.*, "Fiber–wireless integrated mobile backhaul network based on a hybrid millimeter-wave and free-space-optics architecture with an adaptive diversity combining technique, " in *Opt. Lett.*, vol. 41, no. 9, pp. 1909–1912, 2016.

[4] G. Kweon, "Noise Figure of Optical Amplifiers, *" Journal of Korean Phy. Soc.*, vol. 41, no. 5, pp. 617-628, Nov. 2002.

[5] B. Razavi, *Design of Integrated Circuits for Optical Communications*, 1st ed. New York, NY, USA: McGraw-Hill, 2003.

[6] I. Ozkaya *et al.*, "A 64-Gb/s 1.4-pJ/b NRZ Optical Receiver Data-Path in 14-nm CMOS FinFET," in *IEEE Journal of Solid-State Circuits*, vol. 52, no. 12, pp. 3458-3473, Dec. 2017.

[7] E. M. Cherry and D. E. Hooper, "The design of wide-band transistor feedback amplifiers, " *Proc. Inst. Electr. Eng.*, vol. 110, no. 2, pp. 375-389, Feb. 1963.